avirulence gene *avrRpm1* (*Pst* DC3000/*avrRpm1*) but susceptible to *Pst* DC3000 [16]. To visualize the $[Ca^{2+}]_i$ increase during the plant defense signaling, we inoculated bacterial pathogens into the leaves of BRAC-expressing *Arabidopsis* lines. We monitored the changes in $[Ca^{2+}]_i$ during 30-45 and 80-95 minutes after the bacterial inoculation (Figure 5). Increase in $[Ca^{2+}]_i$ was observed at approximate 90 minutes after the inoculation of *Pst* DC3000/*avrRpm1* but not *Pst* DC3000. This result is consistent with the finding performed using aequorin-expressing *Arabidopsis* plants [17]. In that paper, aequorin could monitor $[Ca^{2+}]_i$ change in whole leaves every 5 sec or visualize $[Ca^{2+}]_i$ change in single leaf every 50 minutes. On the other hand, BRAC successfully visualized the $[Ca^{2+}]_i$ change in a region of single leaf every 10 sec.

Discussion

We successfully designed and constructed the BRET-based ratiometric Ca^{2+} indicator, BRAC, which could visualize intracellular Ca^{2+} dynamics with 1-second temporal resolution at the single-cell level. Taking advantage of the bioluminescence imaging property that does not require external excitation light, BRAC is a potentially powerful tool for elucidating the cellular implementation of systems-level neural processes such as action, thought and emotion by combining its use with an optogenetic technology for genetically targeted, millisecond-timescale optical excitation of neurons expressing a light-driven cation channel and pump such as Channelrhodopsin-2, and chloride pump, NpHR, respectively [18].

To date, many FRET-based indicators have been developed [19]. Generally, these

indicators use CFP and YFP as the FRET donor and acceptor, respectively. Given the similar emission spectrum between CFP and RLuc8, we could construct BRET-based indicators simply by substituting RLuc8 for the CFP moiety in the FRET-based indicators. However, this substitution of donor molecule may not yield high-performance indicators with a large dynamic range. To enhance the dynamic range, it may be necessary to use circularly permuted Venus variants to enable optimization of relative orientation between RLuc8 and Venus. Also, the development and application of circularly permuted RLuc8 variants might greatly improve BRET-based indicators in future.

Materials and Methods

Reagents

Coelenterazine-h was purchased from Promega (Madison, WI), Ni-NTA agarose from Qiagen GmbH (Hilden, Germany), Lipofectamine 2000 from Invitrogen (Carlsbad, CA), Dulbecco's Modified Eagle's Medium (DMEM) from Sigma (St. Louis, MO), ionomycin from Calbiochem (San Diego, CA) and fetal bovine serum from BioWest (Nuaillé, France).

Gene construction

pGL4.70 [hRLuc] (Promega) was used as the template for introducing eight mutations, A55T/C124A/S130A/K136R/A143M/M185V/M253L/S287L, by means of a site-directed mutagenesis method to yield RLuc8 [2]. A series of BRET-based Ca^{2+} indicators was constructed by replacing ECFP and cp173Venus in YC3.60 with Venus or circularly permuted Venus variants, and RLuc8, respectively. G5A gene was constructed by fusion of

GFP gene with aequorin coding sequences through 5 times repeating SGGSGSGGQ peptide coding sequence as shown previously [5].

Protein expression, purification and Ca^{2+} titration in vitro

Recombinant BRAC protein with N-terminal polyhistidine tags was expressed in *Escherichia coli* [JM109(DE3)] at 23°C, purified using an Ni-NTA column (Qiagen) and then diluted to 20 nM in 50 mM HEPES, pH 8.0. Emission spectra of BRAC were measured using a spectrophotometer (F-2500; Hitachi) and a microplate reader (SH-9000; Corona Electric). Final concentration of 1–10 μM coelenterazine-h (Promega) was used as the luminescent substrate for RLuc8. Ca^{2+} titration was performed by reciprocal dilution of Ca^{2+}-free and Ca^{2+}-saturated buffers prepared using *O,O'*-bis(2-aminoethyl)ethyleneglycol-*N,N,N',N'*-tetraacetic acid (EGTA), *N*-(2-Hydroxyethyl)ethylenediamine-*N,N',N'*-triacetic acid (EDTA-OH), or Nitrilotriacetic acid (NTA) in 100 mM KCl, 10 mM MOPS (pH 7.2). Free Ca^{2+} concentrations were calculated by using 0.15, 4.3 and 170 μM as the K_d value of EGTA, EDTA-OH and NTA for Ca^{2+}, respectively [20]. A Ca^{2+} titration curve was used to calculate apparent K_d value by non-linear regression analysis. The averaged data from eight independent measurements were fitted to the Hill equation using Origin7 software (OriginLab).

Measurement of Ca^{2+} binding kinetics

Measurements of Ca^{2+} binding kinetics of BRAC were performed by using stopped-flow photometry system consisting of RX.2000 rapid mixing stopped-flow unit (Leatherhead,

UK) and FP-750 spectrophotometer (JASCO, Japan). Emission intensity of Venus (530 nm) from BRAC were monitored at 1 kHz just after rapid mixing of 5 nM BRAC protein with 20 μM coelenterazine-h in various concentration of Ca^{2+} buffer. In this experiment, we did not mix coelenterazine-h with BRAC prior to measurement to avoid undesirable consumption of coelenterazine-h by Rluc8 in BRAC during sample preparation. Thus, time course of emission intensity in the stopped-flow experiments consists of three components of kinetics derived from Ca^{2+} binding to BRAC, coelenterazine-h binding to BRAC, and catalytic oxidation of coelenterazine-h by BRAC. To estimate the catalytic oxidation of coelenterazine-h by Rluc8 in BRAC, we measured time course of emission intensity change after mixing BRAC with 20 μM coelenterazine-h in Ca^{2+}-free solution, and used the obtained data as a "base line". Then, we measured time course of both association and dissociation of Ca^{2+} to and from BRAC by mixing 1 volume of BRAC in Ca^{2+}-free buffer with 25 volume of solution containing 1.69 μM Ca^{2+}, and 1 volulme of BRAC in 1.69 μM Ca^{2+} solution with 25 volume of Ca^{2+}-free buffer, respectively. The averaged data from at least 5 independent measurements were used for following analysis. The averaged time course data for association and dissociation kinetics were subtracted by the base line to remove the fraction derived from autonomous catalytic oxidation of coelenterazine-h by BRAC. Then, the time constants (τ) were calculated by means of curve fitting in single exponential equation using the data from 0.2 sec to 2.0 sec to minimize contribution of signal derived from association of coelenterazine-h with BRAC just after mixing. Measurements of Ca^{2+} binding kinetics of YC3.60 were performed as shown previously [11]. In the stopped-flow experiment, final Ca^{2+} concentration was controlled by reciprocal

dilution of Ca^{2+}-free and Ca^{2+}-saturated buffers prepared using *O,O'*-bis(2-aminoethyl)ethyleneglycol-*N,N,N',N'*-tetraacetic acid (EGTA) in 100 mM KCl, 10 mM MOPS (pH 7.2). Free Ca^{2+} concentration in every solution was confirmed with Ca^{2+}-sensitive electrode (Metrohm, Herisau, Switzerland) which is calibrated with a $CaCl_2$ standard solution (Orion Research, Cambridge, MA).

pH titration

pH titration was performed using a series of 20 mM buffers with 100 mM KCl in pH 5.7 and 6.2 (MES), 6.6 and 7.0 (MOPS), 7.4 (Tris), 7.8 and 8.0 (HEPES), and 8.6 (Glycin).

Cell culture and transfection

Hela cells were cultured in a homemade 35-mm glass-bottom dish in DMEM (Sigma) containing 10% fetal bovine serum (BioWest). Cells were transfected with plasmids by means of Lipofectamine 2000 (Invitrogen). At 1 to 2 days after transfection, cells expressing BRAC or G5A were subjected to imaging. 10 μM coelenterazine-h were added to the culture medium just before observation of BRAC and 1-4 hours before observation of G5A.

Plant growth and pathology test conditions

We used homozygous *Arabidopsis thaliana* (ecotype Columbia, Col-0) expressing BRAC under control of the *35S* promoter. Plants were grown at 22 °C under the 8-h-light in

a day for 5-6 weeks. For pathology tests, we used *Pseudomonas syringae* pv. *tomato* DC3000 (*Pst* DC3000) and an avirulent strain (*Pst* DC3000/*avrRpm1*) that was kindly provided by Dr. Jeffery L. Dangl. We cultured the bacteria in KB medium with kanamycin (30 μg/ml) and rifampicin (100 μg/ml) [21]. After washing the cells twice in 10 mM $MgCl_2$, we suspended them at $5x10^7$ cfu/ml for pathology tests. We inoculated the suspensions into the abaxial surfaces of leaves with needleless syringes.

Live cell Imaging

An inverted microscope (Ti-E, Nikon) was used to observe BRET and G5A signals in living cells maintained at 37°C with a continuous supply of 95% air and 5% carbon dioxide by using a stage-top incubator (Tokai Hit, Fujinomiya, Japan). Light emission from the samples was focused by a 40× oil-immersion objective lens (Nikon Plan Fluor, numerical aperture 1.3) on a cooled electron-multiplying charge-coupled device (EM-CCD) camera (ImagEM; Hamamatsu Photonics). A 2×2 binning setting was used for every 1-second imaging. To simultaneously acquire both RLuc8 and Venus images, we used a W-View system (Hamamatsu Photonics) composed of 510-nm short pass and 510-nm long pass dichroic mirrors, and F01-479/40 and F01-536/40 bandpass filters (both from Semrock) to

split the RLuc8 and Venus images. Image analysis was performed using Aquacosmos (Hamamatsu Photonics). Maximum and minimum BRET ratio values in Hela cells were measured after treatment with 5 μM ionomycin/1 mM EGTA, and 5 μM ionomycin/5 mM Ca^{2+}, respectively.

Live plant imaging

We used macro zoom microscopy (MVX10, Olympus) with 1× objective lens (Olympus MVPLAPO1X, numerical aperture 0.25) on a cooled electron-multiplying charge-coupled device (EM-CCD) camera (iXon DU-897E-BV, Andor Technology). A 1×1 binning setting was used for every 10-second imaging. To simultaneously acquire both RLuc8 and Venus images, we used W-View system and mirrors as aforementioned in section of living cell imaging.

Supporting Information

Supporting Video 1

Video showing cytosolic Ca^{2+} oscillation in HeLa cells expressing BRAC in response to the application of 10 μM hisitamine. Video corresponds to the data in Figure 4D. Resolution is 128x256, Quick-Time, 2.93 MB.

Acknowledgments

This work was partly supported by grants from Scientific Research on Advanced Medical Technology of the Ministry of Labor, Health and Welfare of Japan, and Precursory Research for Embryonic Science and Technology of the Japan Science and Technology Agency. We are grateful to Drs. Jeff L. Dangl at University of North Carolina and Junji Yamaguchi at Hokkaido University for donating *Pst* DC3000 strains.

Author Contributions

Conceived and designed the experiments: TN. Acquired and analyzed the data: KS KH. Wrote the paper: KS TN. Prepared plant and performed plant experiments: NH. Measure the sensor kinetics: TM and KM.

References

1. Hoshino H, Nakajima Y, Ohmiya Y (2007) Luciferase-YFP fusion tag with enhanced emission for single-cell luminescence imaging. Nat Methods 4: 637–639.
2. Loening AM, Fenn TD, Wu AM, Gambhir SS. (2006) Consensus guided mutagenesis of Renilla luciferase yields enhanced stability and light output. Protein Eng Des Sel 19: 391–400.
3. De A, Ray P, Loening AM, Gambhir SS (2009) BRET3: a red-shifted bioluminescence resonance energy transfer (BRET)-based integrated platform for imaging protein-protein interactions from single live cells and living animals. Faseb J 23: 2702–2709.
4. Brini M, Marsault R, Bastianutto C, Alvarez J, Pozzan T, et al. (1995) Transfected aequorin in the measurement of cytosolic CA^{2+} concentration ($[CA^{2+}]_C$). J Biol Chem 270: 9896–9903.

5. Baubet V, Le Mouellic H, Campbell AK, Lucas-Meunier E, Fossier P, et al. (2000) Chimeric green fluorescent protein-aequorin as bioluminescent Ca^{2+} reporters at the single-cell level. Proc Natl Acad Sci 97: 7260–7265.
6. Shimomura O, Kishi Y, Inouye S (1993) The relative rate of aequorin regeneration from apoaequorin and coelenterazine analogs. Biochem J 296: 549–551.
7. Shimomura O (2006) The jellyfish *Aequoria* and other luminous coelenterates. In: Bioluminescence. Singapore: World Scientific. pp. 115-116.
8. Kaihara A, Umezawa Y, Furukawa T (2008) Bioluminescent indicators for Ca^{2+} based on split Renilla luciferase complementation in living cells. Anal Sci 24: 1405–1408.
9. Kim SB, Sato M, Tao H (2009) Split Gaussia luciferase-based bioluminescence template for tracing protein dynamics in living cells. Anal Chem 81: 67–74.
10. Nagai T, Ibata K, Park ES, Kubota M, Mikoshiba K, et al. (2002) A variant of yellow fluorescent protein with fast and efficient maturation for cell-biological applications. Nat Biotechnol 20: 87–90.
11. Miyawaki A, Llopis J, Heim R, McCaffery JM, Adams JA, et al. (1997) Fluorescent indicators for Ca^{2+} based on green fluorescent proteins and calmodulin. Nature 388: 882–887.
12. Nagai T, Yamada S, Tominaga T, Ichikawa M, Miyawaki A (2004) Expanded dynamic range of fluorescent indicators for Ca2+ by circularly permuted yellow fluorescent proteins. Proc Natl Acad Sci 101: 10554–10559.
13. Dacres H, Dumancic MM, Horne I, Trowell SC (2009) Direct comparison of bioluminescence-based resonance energy transfer methods for monitoring of proteolytic cleavage. Anal Biochem 385: 194–202.
14. Nakai J, Ohkura M, Imoto K (2001) A high signal-to-noise Ca2+ probe composed of a single green fluorescent protein. Nat Biotechnol 19: 137-141.
15. Lecourieux D, Ranjeva R, Pugin A (2006) Calcium in plant defence-singalling pathways. New Phytologist 171: 249-269.
16. Mackey D, Holt III BF, Wiig A, Dangl JL (2002) RIN4 interacts with *Pseudomonas* syringae type III effector molecules and is required for RPM1-mediated resistance in *Arabidopsis*. Cell 108: 743-754.

17. Grant M, Brown I, Adams S, Knight M, Ainslie A, et al. (2000) The *PRM1* plant disease resistance gene facilitates a rapid and sustained increase in cytosolic calcium that is neccessary for the oxidative burst and hypersensitive cell death. The Plant J 23: 441-450.

18. Zhang F, Wang LP, Brauner M, Liewald JF, Kay K, et al. (2007) Multimodal fast optical interrogation of neural circuitry. Nature 446: 633–636.

19. Frommer WB, Davidson MW, Campbell RE (2009) Genetically encoded biosensors based on engineered fluorescent proteins. Chem Soc Rev 38: 2833–2841

20. .Tsien RY, Pozzan T (1989) Meausrement of cytosolic free Ca^{2+} with Quin2. Methods Enzymol 172: 230-262

21. Katagiri F, Thilmony R, He SY (2002) The Arabidopsis thaliana-Pseudomonas syringae interaction. In: Somerville C, Meyerowitz E, editors. The Arabidopsis Book. Boston: American Society for Plant Biology. pp. 1-35.

Figure Legends

Figure 1. Schematic structures of yellow cameleon 3.60 (YC3.60) and BRAC derivatives. (**A**) Domain structure of YC3.60 and BRAC derivatives. Circularly permuted Venus variants are indicated as cp50, 157, 173, 195, and 229Venus, which have different translation start sites from the original Venus. (**B**) Schematic three-dimensional structure of BRAC, which is composed of the Ca^{2+}-sensing domain, calmodulin (CaM) and M13, sandwiched between Venus and RLuc8. In the Ca^{2+} free state (left panel), CaM-M13 has an extended conformation so Venus is not located close to RLuc8 and thus only weak emission can be seen from Venus due to low BRET efficiency. Upon Ca^{2+} binding to CaM (right panel), Ca^{2+}-CaM makes a compact complex with M13, which induces efficient

BRET from RLuc8 to Venus resulting in fluorescence emission peaking at 530 nm.

Figure 2. Spectral properties of BRAC derivatives. Emission spectra of BRAC derivatives, (**A-F**) RLuc8-CaM-M13-Venus or cpVenus variants, (**E-J**) Venus or cpVenus variants-CaM-M13-RLuc8, under zero Ca^{2+} (dashed line) and saturated Ca^{2+} (solid line) conditions.

Figure 3. Chemical properties of BRAC. (**A**) Normalized emission spectra of BRAC at indicated free Ca^{2+} concentrations. All spectra were normalized at 480 nm. (**B**) Ca^{2+} titration curve of emission ratio (530 nm/480 nm) in BRAC. (**C**) pH titration curves of BRAC. pH titration curves of BRAC at zero (dashed line) and saturated (solid line) Ca^{2+}. (**D**) Time traces of luminescence intensity of BRAC after the rapid mixing of Ca^{2+}-saturated BRAC with Ca^{2+}-free buffer. A fitted curve of single-exponential function is shown as red lines. (**E**) The dissociation time constant at various Ca^{2+} concentration. (**F**) Relaxation rate constant (k_{obs}) for reaction of YC3.60 with Ca^{2+}. Association rate (k_{on}) and dissociation rate (k_{off}) can be calculated from fitting equation $k_{obs} = k_{on}\,[Ca^{2+}] + k_{off}$ and dissociation constant (K_d) can be calculated from the following equation $K_d = k_{off} / k_{on}$.

Figure 4. Ca^{2+} imaging of Hela cells by using BRAC. (**A**) Fluorescence image of Hela cells expressing BRAC. Emission signal from Venus (**B**) and RLuc8 (**C**). (**D**) A series of

pseudo-colored BRET images showing Ca^{2+} dynamics taken every 1 second. (**E**) Time course of averaged intensity of RLuc8 (gray line) and Venus (black line) at a cell shown in (B). (**F**) Time course of $\Delta R/R_0$ at the same cell. (**G**) Time course of averaged intensity of Hela cell expressing G5A. 10 uM histamine treatment were done at ~100 second. Scale bar, 20 μm.

Figure 5. Ca^{2+} imaging of plant leaves by using BRAC. A series of pseudo-colored BRET images showing Ca^{2+} dynamics in plant leaves 30 minutes (**A**) and 80 minutes (**B**) after inoculation of *Pst* DC3000/*avrRpm1* and *Pst* DC3000 (control). (**C, D**) Time course of $\Delta R/R_0$ at the plant leaves inoculated *Pst* DC3000/*avrRpm1* (black line) and *Pst* DC3000 (gray line). 0 min represents the time of bacteria inoculation. Scale bars, 1 mm.

Table 1. Emission ratio (530 nm/480 nm) without and with Ca^{2+} and dynamic range of newly developed constructs.

Construct	- Ca^{2+}	+ Ca^{2+}	Dynamic range (%)
Rluc8-CaM-M13-cp173Venus	0.8	0.9	10
Rluc8-CaM-M13-Venus	0.8	1.0	30
Rluc8-CaM-M13-cp50Venus	0.5	0.5	0
Rluc8-CaM-M13-cp157Venus	0.9	1.2	30
Rluc8-CaM-M13-cp195Venus	0.7	0.8	10
Rluc8-CaM-M13-cp229Venus	0.7	0.7	0
Venus-CaM-M13-Rluc8	1.1	1.8	60
cp50Venus-CaM-M13-Rluc8	1.2	1.0	20
cp157Venus-CaM-M13-Rluc8	1.1	1.4	20
cp173Venus-CaM-M13-Rluc8	1.1	1.3	10
cp195Venus-CaM-M13-Rluc8	1.1	1.2	10
cp229Venus-CaM-M13-Rluc8	1.1	1.5	30

Figure 1 Saito et al.

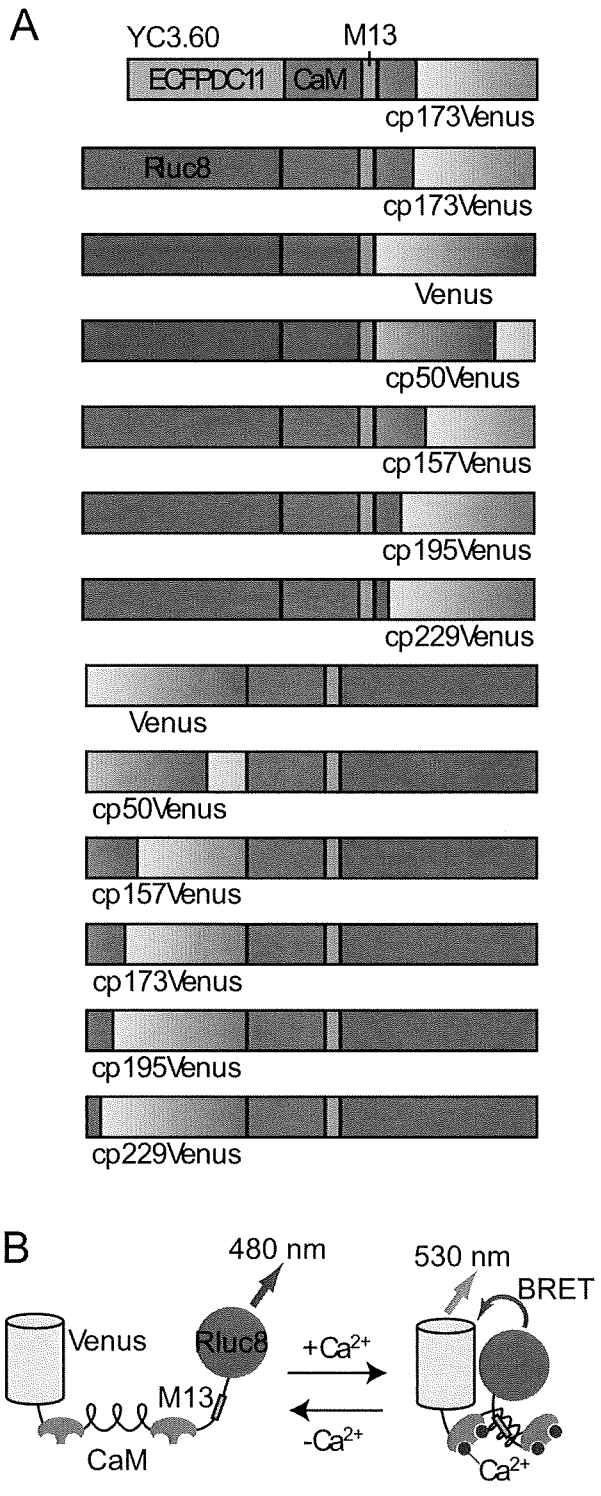

Figure 2 Saito et al.

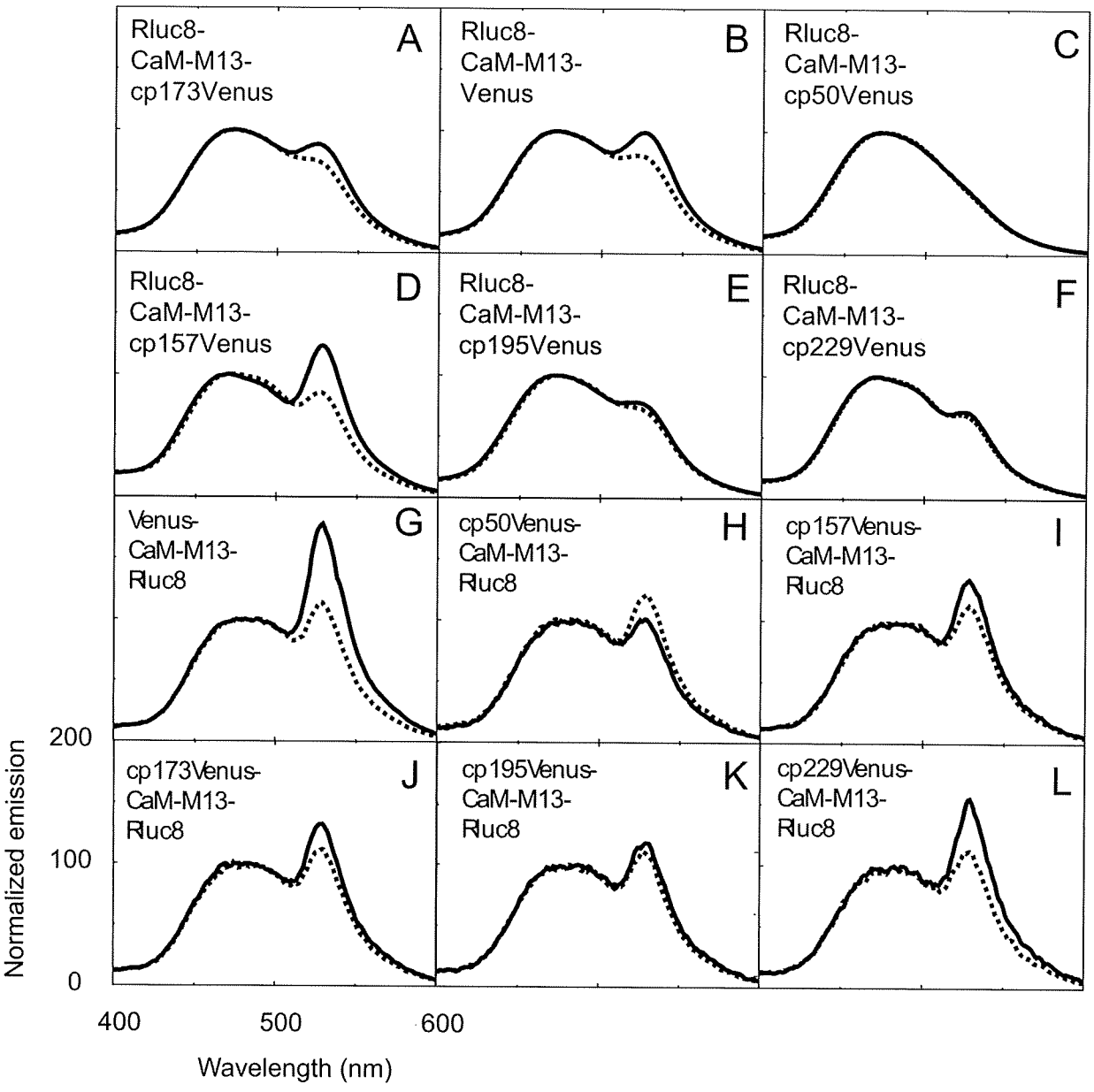

Figure 3 Saito et al.

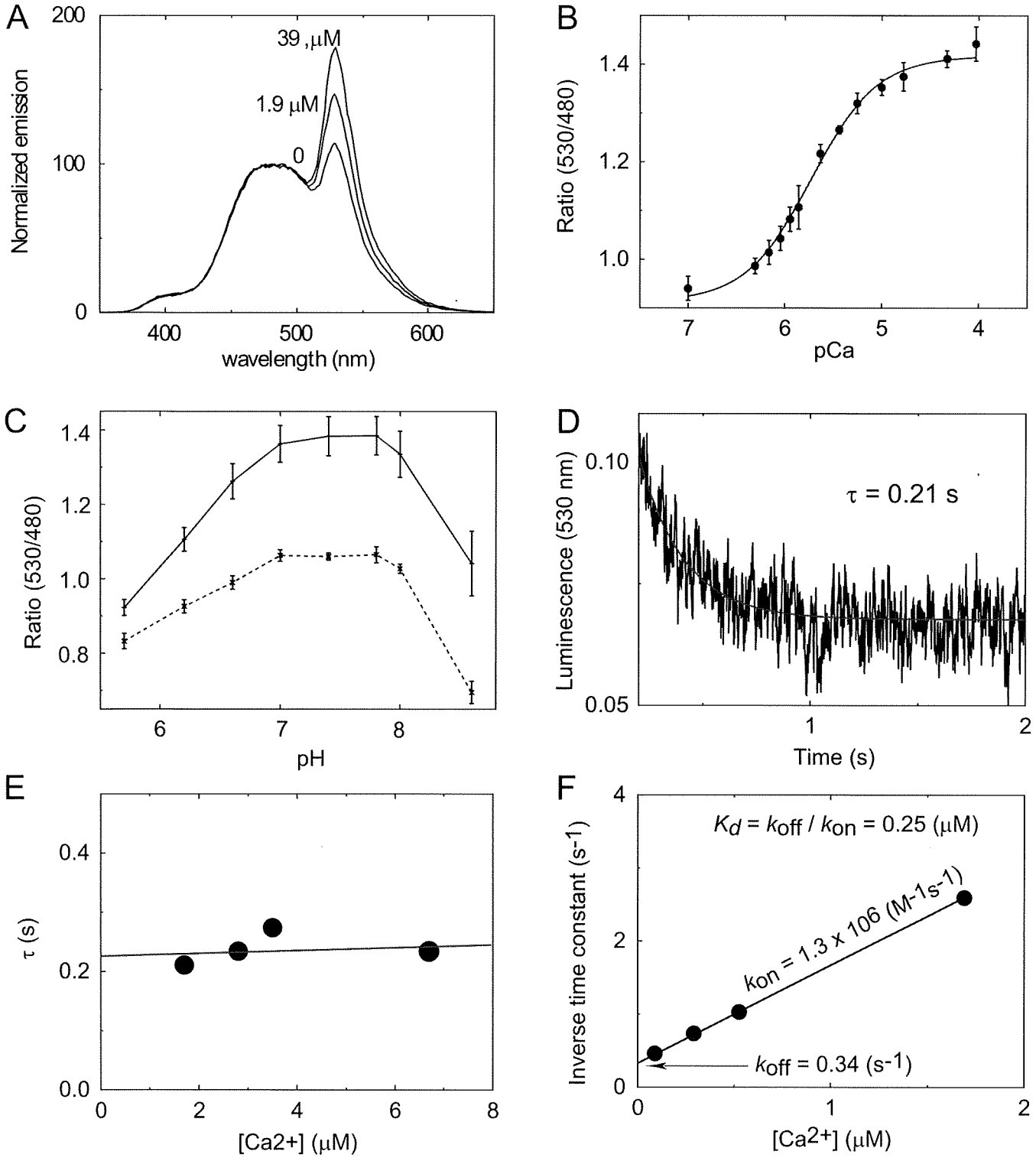

Figure 4 Saito et al.

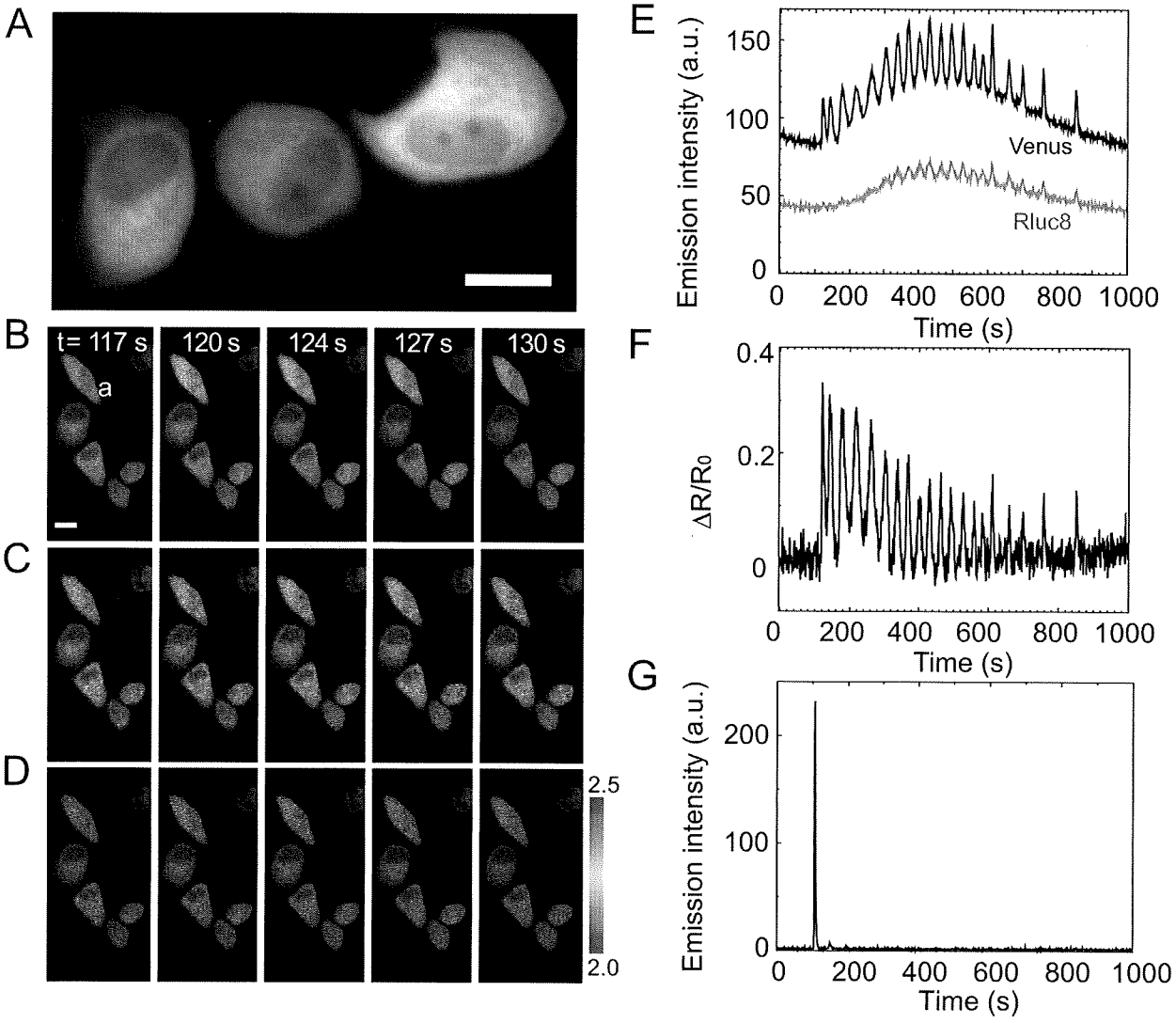

Figure 5 Saito et al.

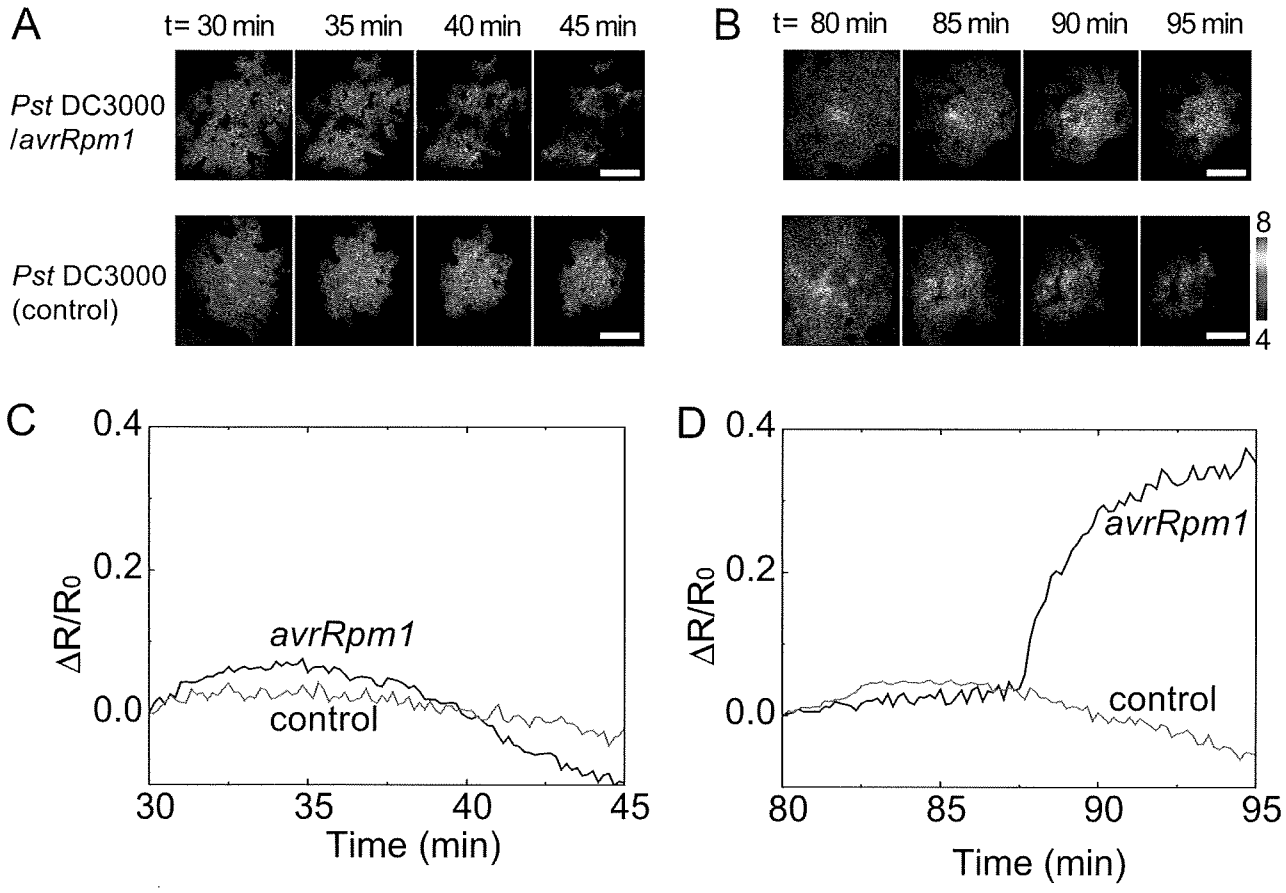

An ultramarine fluorescent protein with increased photostability and pH insensitivity

Wataru Tomosugi[1], Tomoki Matsuda[1], Tomomi Tani[1], Tomomi Nemoto[2], Ippei Kotera[1], Kenta Saito[3], Kazuki Horikawa[3] & Takeharu Nagai[1,3]

We report a pH-insensitive and photostable ultramarine fluorescent protein, Sirius, with an emission peak at 424 nm, the shortest emission wavelength among fluorescent proteins reported to date. The pH-insensitivity of Sirius allowed prolonged visualization of biological events in an acidic environment. Two fluorescence resonance energy transfer (FRET) pairs, Sirius-mseCFP and Sapphire-DsRed, allowed dual-FRET imaging with single-wavelength excitation, enabling detection of Ca^{2+} concentration and caspase-3 activation in the same apoptotic cells.

Among the fluorescent proteins reported to date, the variant with a Phe66 mutation in wild-type *Aequorea Victoria* GFP has the shortest emission wavelength, with a peak at 442 nm[1]. However, fluorescence quantum yield of the GFP-Phe66 variant is low ($\Phi_{Fl} = 0.013$), strictly limiting its applicability for bioimaging.

To evolve the dim GFP-Phe66 mutant into a bright fluorescent protein, we randomly mutagenized the sequence encoding four amino acids surrounding the chromophore of mseCFP-W66F, which had been made by introducing the W66F mutation into the cyan fluorescent protein variant, mseCFP (ref. 2) (**Table 1** and **Supplementary Fig. 1** online). One resulting protein containing four substitutions (T65Q, Y145G, H148S and T203V; **Supplementary Fig. 1**) was an ultramarine fluorescent protein with a 25-fold increase in fluorescence intensity (**Fig. 1a** and **Supplementary Fig. 2** online). This protein, UMFP-1, had an emission peak at 424 nm and a bimodal absorption peak at 280 and 355 nm (**Fig. 1b**). Owing to its greatly blue-shifted spectrum, UMFP-1 was spectrally compatible for multicolor imaging with CFP, YFP and RFP (**Fig. 1c** and **Supplementary Fig. 3** online). UMFP-1 could also be used in a detection channel distinct from BFP, for extended multicolor imaging by linear spectral unmixing (**Supplementary Fig. 4** online).

To improve the brightness of UMFP-1, we introduced an F46L mutation into the protein, yielding UMFP-2; this mutation promotes chromophore maturation at 37 °C (ref. 3). Then, we conducted two more rounds of random mutagenesis on the entire gene using error-prone PCR and obtained still-brighter mutants UMFP-3 (UMFP-2–Q69L) and UMFP-4 (UMFP-3–F223S) (**Supplementary Fig. 1**). The final variant, UMFP-4, which we named Sirius, had 80-fold brighter fluorescence than mseCFP-W66F and the same spectrum as UMFP-1 (**Table 1** and **Supplementary Fig. 2**). These increases in fluorescence intensity were mainly due to improvements in Φ_{Fl} (**Table 1**).

Notably, although Sirius had a smaller absorption coefficient (ε) and Φ_{Fl} than the BFPs, its fluorescence intensity in bacterial cells at 37 °C was about twice that of EBFP and two-thirds of EBFP2 (ref. 4) (**Supplementary Fig. 5a** online). We also observed a similar fluorescence intensity in mammalian cells (**Supplementary Fig. 5b**), suggesting that the Sirius chromophore underwent

Table 1 | Physical and optical properties of ultramarine fluorescent proteins variants

Protein	Color	λ_{ab}[a] (nm)	λ_{em}[b] (nm)	ε ($M^{-1}cm^{-1}$)	Φ_{Fl}	pKa	τ_{bleach}[c] (arc lamp)	τ_{bleach} (laser)	Φ_{bleach} ($\times 10^{-6}$)	Relative fluorescence[d] *Escherichia coli*	Relative fluorescence[d] HEK293	K_{ox}[e] ($\times 10^{-4}$ s^{-1})
mseCFP	Cyan	434	474	30,000	0.4	6.4	–	–	–	–	–	–
mseCFP-W66F	Ultramarine	355	424	14,000	0.003	–	–	–	–	–	–	–
UMFP-1	Ultramarine	355	424	15,000	0.07	<3.0	–	–	–	–	–	–
UMFP-2	Ultramarine	355	425	15,000	0.11	<3.0	–	–	–	–	–	–
UMFP-3	Ultramarine	355	424	13,000	0.16	<3.0	–	–	–	–	–	–
UMFP-4 (Sirius)	Ultramarine	355	424	15,000	0.24	<3.0	62	7.3	9.79	2.2	1	5.6
EBFP2	Blue	380	447	34,000	0.54	5.7	13	9.9	5.12	2.8	1.8	4.4
EBFP	Blue	380	448	32,000	0.25	6.3	1	1	113	1	1	4.7

[a]Absorption wavelength peak. [b]Emission wavelength peak. [c]Time needed to bleach 1/e of maximum fluorescence intensity in HeLa cells ($n = 3$) relative to EBFP. [d]Fluorescence intensity relative to that of EBFP in *E. coli* and HEK293 at 37 °C. The amount of protein in *E. coli* was estimated by measuring absorption at 600 nm. The amount of protein in HEK293 was determined by western blotting with antibody to GFP. [e]Time constant of oxidation. –, not determined.

[1]Laboratory for Nanosystems Physiology, Research Institute for Electronic Science, Hokkaido University, Sapporo, Hokkaido, Japan. [2]Supportive Center for Brain Research, National Institute for Physiological Science, Okazaki, Aichi, Japan. [3]Nikon Imaging Center, Research Institute for Electronic Science, Hokkaido University, Sapporo, Hokkaido, Japan. Correspondence should be addressed to T. Nagai (tnagai@es.hokudai.ac.jp).

RECEIVED 2 JANUARY; ACCEPTED 12 FEBRUARY; PUBLISHED ONLINE 6 APRIL 2009; DOI:10.1038/NMETH.1317

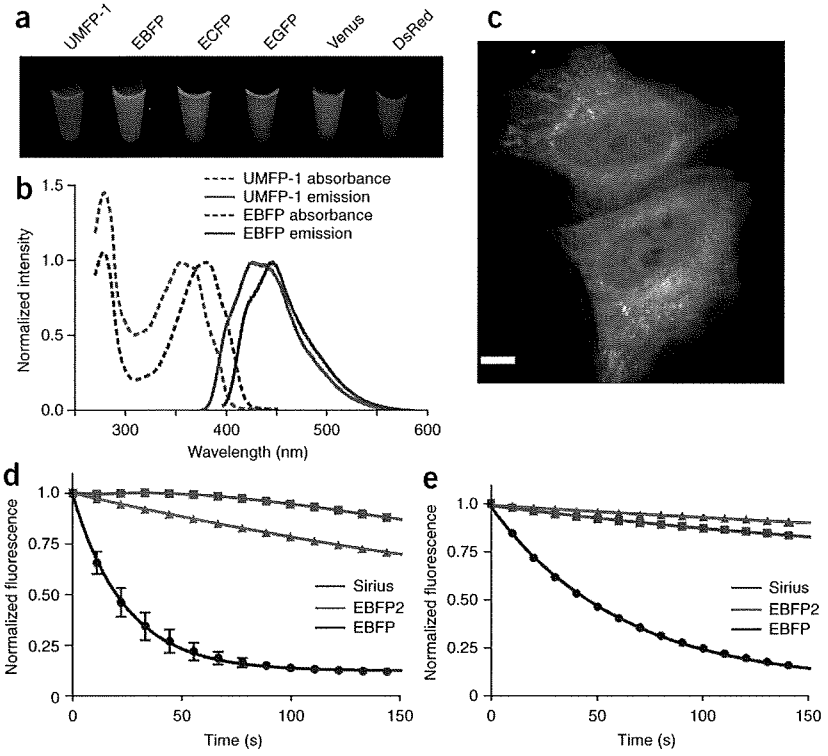

Figure 1 | Characterization of UMFP variants. (**a**) Fluorescence of purified UMFP-1 and conventional fluorescent proteins, with 365-nm excitation. (**b**) Absorption and emission spectra of UMFP-1 and EBFP. (**c**) Multicolor imaging of HeLa cells with UMFP-1–labeled nuclei (red), mseCFP–labeled endoplasmic reticulum (cyan), Venus–labeled mitochondria (yellow) and mCherry–labeled microtubules (magenta). Scale bar, 10 μm. (**d**,**e**) Photobleaching curves of Sirius, EBFP2 and EBFP in HeLa cells, excited by a mercury arc lamp through a 352-nm–388-nm excitation filter (**d**) and using a 375-nm diode laser (**e**). All curves were normalized to the fluorescence intensity before photobleaching. Error bars, s.d. ($n = 3$).

efficient post-translational maturation in the intracellular environment at 37 °C. Concordantly, the rate of Sirius's chromophore oxidation, which is the rate-limiting step of chromophore formation, was larger than that for either EBFP or EBFP2 (**Table 1** and **Supplementary Fig. 5c**).

Because one of the mutated amino acids (F223S) in Sirius faced outside of the protein, it was possible that Sirius had different oligomerization properties than mseCFP. However, the fluorescence signal of Sirius expressed in HeLa cells was evenly distributed in the cytoplasm and nucleus without any visible aggregates or nonspecific localization (**Supplementary Fig. 6a** online), suggesting that it is a monomer, although this would need to be confirmed by additional analysis. Sirius fusions did not perturb the localization of several fusion partners (**Supplementary Fig. 6b–i**); an exception was the fusion of Sirius with α-tubulin, which localized to microtubules but was also found in the cytoplasm (data not shown). Optimization of amino acid linker length between Sirius and α-tubulin may improve the localization.

When compared with EBFP and EBFP2 in HeLa cells, the photobleaching kinetics of Sirius using a mercury arc lamp was 62 times and 5 times slower than that of EBFP and EBFP2, respectively (**Fig. 1d** and **Table 1**). Furthermore, although the bleaching curves of EBFPs showed single exponential decay, those of Sirius exhibited two components: a flat, stable component followed by exponential decay, suggesting a complicated bleaching process (**Fig. 1d**). However, we observed simple exponential decay for both Sirius and EBFP2 when they were bleached by an intense 375 nm laser. (**Fig. 1e** and **Table 1**). We also calculated the quantum yield for photobleaching (Φ_{bleach}) that does not depend on the absorption coefficient (ε) of each fluorescent protein (**Table 1** and **Supplementary Methods** online). Φ_{bleach} of Sirius (9.79×10^{-6}) was much smaller than that of EBFP (1.13×10^{-4}) and comparable to that of EBFP2 (5.12×10^{-6}).

The most noteworthy feature of Sirius is its fluorescence stability in a wide range of proton concentrations (pH 3–9) (**Fig. 2a**). Presumably, this is due to the Phe66 mutation of the chromophore, as the resulting benzyl, unlike phenol, has no ionizable group. This pH-insensitivity of Sirius may make it highly suitable for fluorescence imaging in acidic environments, such as in phagosomes. We observed phagocytosis of fluorescent protein–expressing bacteria by *Dictyostelium discoidium*. We used two-photon excitation by a 780-nm pulse laser to minimize photodamage induced by wide-field UV-light excitation of the highly photosensitive *Dictyostelium*

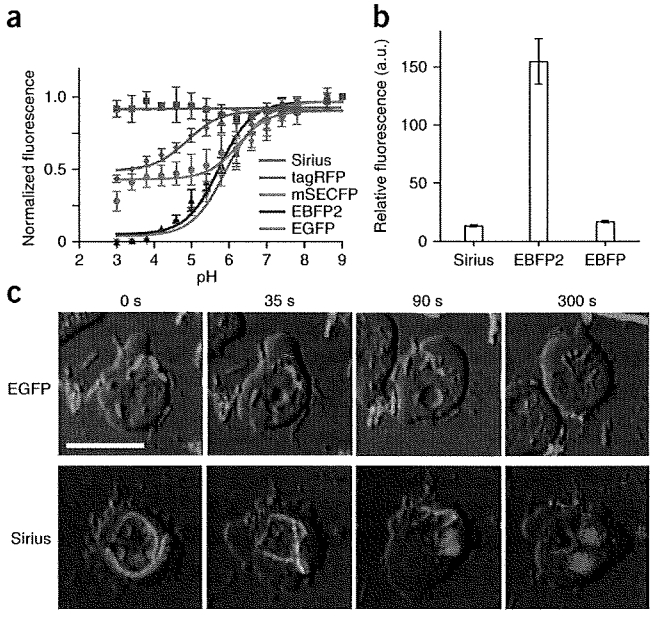

Figure 2 | pH-sensitivity of Sirius. (**a**) pH dependence of the fluorescence emission of the indicated purified proteins. Data are mean ± s.d. ($n = 3$). (**b**) Mean fluorescence intensity of the indicated proteins expressed in HeLa cells ($n = 30$), under two-photon excitation at 780 nm. Error bars, s.e.m. (**c**) Differential interference contrast images merged with corresponding fluorescence images, monitoring phagocytosis of fluorescent protein–expressing bacteria by *Dictyostelium discoidium* at the indicated times. Scale bar, 5 μm.